Evidence for Water Binding to the Fe Center in Cytochrome P450cam Obtained by ^{17}O Electron Spin Echo Envelope Modulation Spectroscopy

H. Thomann,*,† M. Bernardo,† D. Goldfarb,*,‡ P. M. H. Kroneck,§ and V. Ullrich§

Contribution from the Exxon Research and Engineering Co., Route 22 East, Annandale, New Jersey 08801, Department of Chemical Physics, The Weizmann Institute of Science, Rehovot 76100, Israel, and Faculty of Biology, University of Konstanz, Universitätstrasse 10, D-78434 Konstanz, Germany

Received March 17, 1995⊗

Abstract: Orientation selective and multiple frequency ESEEM experiments on substrate free cytochrome P450cam (CP450cam) with ^{17}O-enriched water are reported. The ^{17}O ESEEM frequencies were obtained from Fourier transformation of the ratio of ESEEM waveforms of CP450cam with enriched water and CP450cam with non-enriched water. Numerical simulations were carried out to determine the isotropic and the anisotropic hyperfine interactions and the quadrupole interaction of the ^{17}O. From the magnitude (e^2qQ/h = 6.6 MHz) and asymmetry (η = 0.95) of the ^{17}O quadrupole interaction, we conclude that the distal axial ligand of Fe^{3+} in the CP450 heme is a water molecule. Moreover, from the orientation of the ^{17}O quadrupole tensor, the orientation of the water molecule was found to be confined (within ±10°) with respect to the Fe–N directions within the heme plane. Two possible sets of isotropic and anisotropic components of the ^{17}O hyperfine interaction, (±2.6, ±0.3 MHz) and (±0.4, ±1.8 MHz), were found to satisfactorily reproduce the experimental results. Both sets indicate very small ^{17}O hyperfine couplings which is consistent with the unpaired electron residing predominately in the d_{yz} orbital of the Fe^{3+}. Ligand field models for each set are presented.

Introduction

The enzymes in the cytochrome P-450 family (CP450) are ubiquitous and remarkably versatile O_2-activating catalysts which belong to the *b*-type heme proteins.[1] CP450 are key enzymes of the biological oxidative metabolism that incorporate one of the oxygen atoms of dioxygen into a broad variety of organic substrates.[2–4] The best characterized CP450 enzyme is the soluble camphor-metabolizing P-450cam isolated from *Pseudomonas putida* (CP450cam). The crystal structure of several forms of CP450cam were determined by Poulos and co-workers.[5–9] These include the crystal structure of the substrate free enzyme,[5] the camphor bound enzyme,[6,7] the ternary complex of CP450cam with carbon monoxide and camphor,[8] and CP450cam bound to the alternative substrates, norcamphor and adamantanone.[9] Recently the crystal structure of another CP450 enzyme, P450BM-3, a bacterial fatty acid monooxygenase from *Bacillus megaterium*, was reported.[10]

The wealth of crystallographic, spectroscopic, and biochemical data available on P450cam advanced significantly the understanding of the mechanism of O_2 activation and electron transfer in CP450 as recently summarized by Poulos and Raag.[11] The first step in the reaction cycle of P450cam is the binding of the substrate which causes changes in the coordination sphere and spin state of the Fe^{3+} ion along with a reduction of the redox potential.[12] In the substrate free CP450cam the iron is hexacoordinated low-spin Fe^{3+}, experiencing a strong ligand field.[5,12] Upon substrate binding, the Fe^{3+} becomes high spin and pentacoordinated which is accompanied by a displacement of the Fe^{3+} from the porphyrin core toward the fifth ligand.[7,12] This proximal axial ligand is a thiolate sulfur from a cysteine residue and remains attached to the Fe^{3+}.[5,7] Possible mechanisms relating the substrate binding, the coordination number, the spin state equilibrium, and the redox potential were discussed by Poulos and Raag.[9,11]

The identity of the sixth (distal) ligand has been a matter of debate for a long time.[13] In the camphor free CP450cam, the heme pocket is occupied by a network of water molecules which are removed from the active site when camphor binds.[14] The X-ray crystal structure of substrate free P450cam obtained at a resolution of 2.2 Å established that the distal ligand is either a water molecule or a hydroxide ion with a Fe–O distance of 2.28 Å.[6] The distal ligand plays an important role in the first step of the CP450 reaction cycle. It appears to modulate the

* Author to whom correspondence should be addressed.
† Exxon Research and Engineering Co.
‡ The Weizmann Institute of Science. Work performed while on sabbatical leave at Exxon from 8/92 to 8/93.
§ University of Konstanz.
⊗ Abstract published in *Advance ACS Abstracts*, July 15, 1995.

(1) (a) Hayaishi, O. *Molecular Mechanisms of Oxygen Activation*; Academic Press: New York, 1974. (b) Sato, R.; Omura, T. *Cytochrome P-450*; Academic Press: New York, 1979.
(2) Coon, M. J.; White, R. E. *Dioxygen Binding and Activation by Metal Centers*; Spiro, T., Ed.; John Wiley and Sons: New York, 1980; pp 73–123.
(3) Murray, R. I.; Fisher, M. T.; Debrunner, P. G.; Sligar, S. G. *Metalloproteins*; Harrison, P. M., Ed.; Verlag Chemie: Basel, 1985; Vol. I, pp 157–206.
(4) Dawson, J. H. *Science* **1988**, *240*, 433.
(5) Poulos, T. L.; Finzel, B. C.; Howard, A. J. *Biochemistry* **1986**, *25*, 5314.
(6) Poulos, T. L.; Finzel, B. C.; Gunsalus, I. C.; Wagner, G. C.; Kraut, J. *J. Biol. Chem.* **1985**, *260*, 16122.
(7) Poulos, T. L.; Finzel, B. C.; Howard, A. *J. Mol. Biol.* **1987**, *195*, 687.
(8) Raag, R.; Poulos, T. L. *Biochemistry* **1989**, *28*, 7586.
(9) Raag, R.; Poulos, T. L. *Biochemistry* **1989**, *28*, 917.
(10) Ravichandran, K. G.; Boddupalli, S. S.; Haseman, C. A.; Peterson, J. A.; Deisenhofer J. *Science* **1993**, *261*, 731.
(11) Poulos, T. L.; Raag, R. *FASEB J.* **1992**, *6*, 674.
(12) Fisher, T. M.; Sligar, S. G. *J. Am. Chem. Soc.* **1983**, *105*, 3754.
(13) Weiner, L. M. *CRC Crit. Rev. Biochem.* **1986**, *20*, 139 and references therein.
(14) Di Primo, G.; Hui, Bon Hoa; Douzou, P.; Sligar, S. G. *Eur. J. Biochem.* **1992**, *209*, 583.

0002-7863/95/1517-8243$09.00/0

changes in spin state, redox potential, and rate of oxidation of the metal center.[15] It is therefore important to unambiguously determine the identity of the distal ligand in substrate free CP450. Moreover, electronic information regarding the Fe−O bond is necessary for understanding why the Fe^{3+} in the substrate free enzyme is low spin.

Information regarding the bonding characteristics of Fe−O can be obtained from the hyperfine coupling of the ligand proton(s). Room temperature NMR relaxation measurements on substrate free P450cam showed a significant enhancement of the water proton relaxation.[16] Interpretation of the relaxation data indicated the presence of one or more strongly exchangeable protons within 2.6−2.9 Å from the heme iron with an isotropic hyperfine constant of 2.2−3.1 MHz.[17] Electron nuclear double resonance (ENDOR) measurements also indicated the existence of strongly coupled exchangeable proton(s) with hyperfine splittings that are in agreement with the NMR results.[18] The possibility that the signal is due to proton(s) bound to the cysteinyl sulfur could not, however, be ruled out.[18] In a recent communication[19] two broad ENDOR peaks corresponding to proton couplings of 12 and 19 MHz were interpreted as originating from two different H_2O ligands in two major conformational substates of the H_2O cluster in the distal heme pocket.

Information regarding the binding and identity of the distal axial ligand can also be derived from the hyperfine and quadrupole interactions of ^{17}O in enriched water. Previous EPR measurements on low-spin CP450cam with $H_2{}^{17}O$ did not show any resolved superhyperfine splittings, although a slight broadening, as compared with non-enriched water, was observed.[20] We therefore applied electron spin−echo envelope modulation (ESEEM) spectroscopy which is particularly useful for the determination of superhyperfine and quadrupole couplings in orientationally disordered systems.[21-23] ESEEM spectroscopy has emerged as an effective technique for the identification of the coordination sphere of active sites in metalloenzymes and metalloproteins.[21,22] In most studies the ESEEM signals originated from $^{14}N/^{15}N$ in nitrogen-containing ligands or from D_2O.[22,24,25] While the information contained in ^{17}O ESEEM is most significant, it is difficult to extract due to the high spin ($I = {}^5/_2$) of ^{17}O, its low gyromagnetic ratio, and its large quadrupole moment. This leads to a rather complicated nuclear Hamiltonian and a considerable inhomogeneous broadening in orientationally disordered systems.[26]

In this paper we present orientation selective ESEEM experiments on substrate free P450cam with ^{17}O-enriched water from which we obtained both the isotropic and the anisotropic hyperfine interactions and the quadrupole interaction of the ^{17}O. From these results we conclude that the axial ligand is a water molecule rather than an hydroxide ion. We also present a molecular bonding model that explains the magnitude and orientation of the ^{17}O hyperfine and quadrupole interactions.

Theoretical Background

The spin Hamiltonian describing a $S = {}^1/_2$, $I = {}^5/_2$ spin system is

$$\mathcal{H} = \frac{\beta}{h}\vec{H}\cdot\mathbf{g}\cdot\vec{S} - \frac{g_n\beta_n}{h}\vec{H}\cdot\vec{I} + \vec{S}\cdot\mathbf{A}\cdot\vec{I} + \vec{I}\cdot\mathbf{Q}\cdot\vec{I} \qquad (1)$$

where **A** and **Q** are the hyperfine and nuclear quadrupole tensors, respectively. **A** is described in terms of its isotropic part a_{iso} and the principal components of its anisotropic part (assumed to be axially symmetric), $-a_\perp$, $-a_\perp$, and $2a_\perp$, and the polar angles θ_I ϕ_I relating its principal axis system (x', y', z') with that of the g matrix (x, y, z). **Q** is expressed in terms of the its principal components, $Q_{zz} = 3/4\{e^2qQ/[I(2I-1)h]\}$, $Q_{xx} = -{}^1/_2Q_{zz}(1-\eta)$, $Q_{yy} = -{}^1/_2Q_{zz}(1+\eta)$, where η is the tensor asymmetry parameter given by $|(Q_{xx} - Q_{yy})/Q_{zz}|$ and the Euler angles α, β, and γ transforming the principal axes system of **Q**, (x'', y'', z''), to that of the g matrix. The orientation of the external magnetic field with respect to the g tensor is given by θ_0 and ϕ_0. In orientation-selective ESEEM carried out on orientationally disordered systems only selected values of θ_0 and ϕ_0 actually contribute to the echo. These values are determined by the position of the resonant magnetic field within the EPR powder pattern line shape.

After diagonalizing the electronic Zeeman term and neglecting the off-diagonal terms $I_iS_{x,y}$, $i = x, y, z$, the above spin Hamiltonian takes a block diagonal form.[27] Each block represents a nuclear Hamiltonian, $\mathcal{H}_{\alpha,\beta}$, corresponding to the two different electron spin manifolds, given by

$$\mathcal{H}_{(\alpha,\beta)} = \pm\frac{1}{2}\frac{\beta}{h}g_{eff}H_0 - \frac{g_n\beta_n}{h}H_0I_z \pm \frac{1}{2}cI_z \pm \frac{1}{2}bI_y \pm \frac{1}{2}aI_x + \vec{I}\cdot\mathbf{Q}\cdot\vec{I} \qquad (2)$$

where

$$c = A_{zx}\sin\theta\cos\phi + A_{zy}\sin\theta\sin\phi + A_{zz}\cos\theta$$

$$b = A_{yx}\sin\theta\cos\phi + A_{yy}\sin\theta\sin\phi + A_{yz}\cos\theta$$

$$a = A_{xx}\sin\theta\cos\phi + A_{xy}\sin\theta\sin\phi + A_{xz}\cos\theta$$

The A_{ij}'s are the elements of the **A** tensor; ϕ and θ are given by[28]

$$\cos\theta = \frac{g_3\cos\theta_0}{g_{eff}}$$

$$\cos\phi = \frac{g_2\sin\theta_0\cos\phi_0}{(g_2{}^2\sin^2\theta_0\sin^2\phi_0 + g_1{}^2\sin^2\theta_0\cos^2\phi_0)^{1/2}}$$

$$\sin\phi = \frac{g_2\sin\theta_0\sin\phi_0}{(g_2{}^2\sin^2\theta_0\sin^2\phi_0 + g_1{}^2\sin^2\theta_0\cos^2\phi_0)^{1/2}}$$

$$g^2{}_{eff} = g_3{}^2\cos^2\theta_0 + g_2{}^2\sin^2\theta_0\sin^2\phi_0 + g_1{}^2\sin^2\theta_0\cos^2\phi_0$$

Once the spin Hamiltonian can be expressed in terms of two nuclear Hamiltonians the two- and three-pulse ESEEM can be computed from the eigenvalues and eigenvectors of $\mathcal{H}_{\alpha,\beta}$ using the general expressions derived by Mims.[27]

(15) Rein, H.; Ristau, O.; Misselwitz, R.; Buder, E.; Ruckpaul, K. *Acta Biol. Med. Ger.* **1979**, *38*, 187.
(16) Griffin, B. W.; Peterson, J. A. *J. Biol. Chem.* **1975**, *250*, 6445.
(17) Philson, S. B.; Debrunner, P. G.; Schmidt, P. G.; Gunsalus, I. C. *J. Biol. Chem.* **1979**, *254*, 10173.
(18) LoBrutto, R.; Scholes, C. P.; Wagner, G. C.; Gunsalus, I. C.; Debrunner, P. G. *J. Am. Chem. Soc.* **1980**, *102*, 1167.
(19) Fann, Y.-C.; Gerber, N. C.; Osmulski, P. A.; Hager, L. P.; Sligar, S. G.; Hoffman, B. M. *J. Am. Chem. Soc.* **1994**, *116*, 5989.
(20) Kroneck, P. M. H. Unpublished results.
(21) Mims, W. B.; Peisach, J. *Advance EPR Techniques, Applications in Biology and Biochemistry*, Hoff, A. J., Ed.; Elsevier: Amsterdam, 1989; Chapter 1.
(22) Dikanov, S. A.; Tsvetkov, Yu. D. *Electron Spin Echo Envelope Modulation (ESEEM) Spectroscopy*; CRC Press Inc.: Boca Raton, FL, 1992.
(23) Kevan, L.; Bowman, M. K., Eds. *Modern Pulsed and Continuous wave Electron Spin Resonance*; Wiley: New York, 1990.
(24) Mims, W. B.; Davis, J. L.; Peisach, J. *Biophys. J.* **1984**, *45*, 755.
(25) McCracken, J.; Peisach, J.; Dooley, D. D. *J. Am. Chem. Soc.* **1987**, *109*, 4064.
(26) Matar, K.; Goldfarb, D. *J. Chem. Phys.* **1992**, *96*, 6464.
(27) Mims, W. B. *Phys. Rev. B* **1972**, *5*, 2409; **1972**, *6*, 3543.
(28) Atherton, N. M. *Electron spin resonance theory and application*; Wiley: New York, 1973; Chapter 7.

When several nuclei contribute to the modulation, the two-pulse echo intensity is

$$V(\tau) = [\prod_{i=1}^{N} V_i(\tau)]\, F(\tau) \qquad (3)$$

$V_i(\tau)$ is the echo amplitude for nucleus i, and $F(\tau)$ represents the echo decay due to the electron spin relaxation.[27] Similarly, the three-pulse echo amplitude for several nuclei is[22]

$$V(\tau,T) = \frac{1}{2}[\prod_{i=1}^{N} V_i^{\alpha}(\tau,T) + \prod_{i=1}^{N} V_i^{\beta}(\tau,T)]\, F(T)\, F(\tau) \qquad (4)$$

The above expressions are correct within the limit that the interaction between the nuclei is negligible.

The four heme nitrogens, ligand protons, and matrix protons all contribute to the modulation resulting in a rather complex ESEEM spectrum with a relatively large number of peaks. It is therefore difficult to identify the ^{17}O modulation frequencies. Isolation of the ^{17}O peaks can be achieved by taking the ratio of the ESEEM of CP450 with $H_2{}^{17}O$ and that of CP450 with H_2O, acquired under identical conditions. Such a methodology has been previously used to analyze ^2H modulation.[24,29]

It is clear from Eqs 3 and 4 that in the case of two-pulse ESEEM, the ratio includes only the ^{17}O modulation whereas in the case of the three-pulse ESEEM the ratio should in principle include residual frequencies corresponding to the other nuclei and their combinations. The intensities of these are, however, very small and can be neglected. Hence, in practice the ^{17}O frequencies can be obtained from the ratio of three-pulse ESEEM spectra as well.

Experimental Section

a. Sample Preparation. Substrate free CP450cam was purified according to procedure described by Gunsalus and Wagner.[30] The CP450cam as isolated contained both high- and low-spin Fe^{3+} in approximately equal amounts. The low-spin form could be separated by passage over a G15 Sephadex column (0.25 mM protein in 0.3 M Tris/HCl, pH 7.5). Two aliquots were freeze dried and added to either 0.25 mL of enriched $H_2{}^{17}O$ (64%) or 0.25 mL of natural abundance H_2O, hereafter called CP450($H_2{}^{17}O$) and CP450(H_2O), respectively. Both samples were analyzed by continuous-wave X-band EPR spectroscopy at 15 K and showed the characteristic rhombic powder pattern of low-spin Fe^{3+} CP450.[31]

b. ESEEM Measurements. The ESEEM measurements were carried out on a home-built spectrometer described elsewhere.[32] The measurements were performed at 1.2 K at two different spectrometer frequencies, 9.06 and 10.6 GHz. The duration of the microwave pulses for the two-pulse ESEEM measurements ($\pi/2 - \tau - \pi - \tau -$ echo) was 30 and 50 ns, respectively, and in the three-pulse experiment ($\pi/2 - \tau - \pi/2 - T - \pi/2 - \tau -$ echo) they were all set to 30 ns. Phase cycling was employed to eliminate unwanted signals from the three-pulse ESEEM.[33] Typically a power of about 50 W was used and the repetition rate was 50 Hz. The spectra of the enriched and non-enriched samples were recorded under the same conditions.

The ^{17}O FT-ESEEM spectra were obtained from the ratio of the corresponding ESEEM waveforms. Prior to Fourier transformation (FT) the background decay was removed using a low pass filter. The FT-ESEEM spectra shown are the cosine spectra after phase correction, required due to spectrometer dead time.

c. Simulations. The simulations were carried out as described in the theoretical background section and the eigenvectors and eigenvalues of the two nuclear Hamiltonians were obtained by numerical diagonalization. The range of orientations (θ_0, ϕ_0) selected by the microwave pulse was determined by simulating the EPR spectrum and searching for all the g-tensor orientations that give rise to an absorption at $H_0 \pm 0.5\Delta$, where Δ corresponds to the EPR inhomogeneous line width and H_0 is the external magnetic field at which the experiment was performed. For each orientation we used a weighting function, $G(\theta_0,\phi_0,H)$ given by

$$G(\theta_0,\phi_0,H) = e^{-0.5[(H_0 - H)/\sigma]^2} \sin\theta_0\, d\theta_0\, d\phi_0 \qquad (5)$$

where $\sigma = \Delta/2.345$. Prior to Fourier transformation the "dc" background was removed and the data were convoluted with a decaying exponential e^{-t/t_0}, where $t = \tau$ or $t = T + \tau$ for two- and three-pulse ESEEM, respectively, and $t_0 = 3$ μs, to account for nuclear and electronic relaxation.

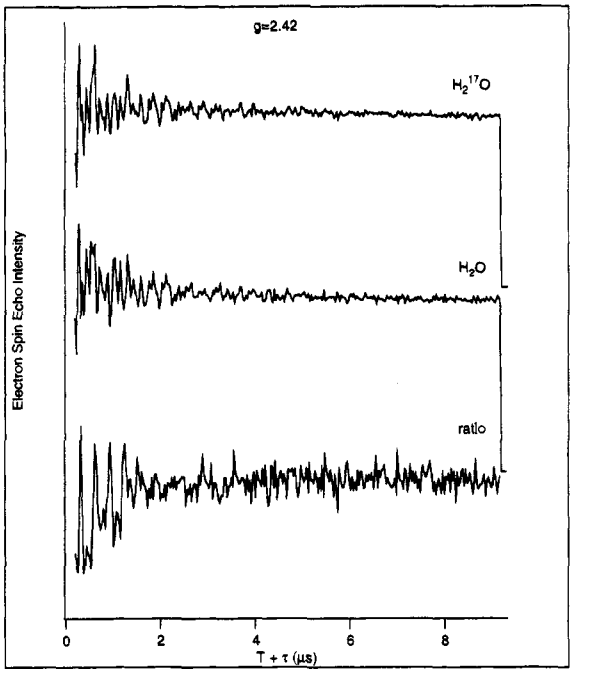

Figure 1. Three-pulse ESEEM waveforms of CP450($H_2{}^{17}O$) and CP450(H_2O) and their ratio, recorded at $g = 2.42$, $H_0 = 2700$ G, and a spectrometer frequency of 9.06 GHz and $\tau = 0.14$ μs.

Results

The EPR spectrum of low-spin CP450 is a typical powder pattern of a $S = {}^1/_2$ spin system with a nonaxial g-tensor where $g_1 = 1.91$, $g_2 = 2.26$, and $g_3 = 2.45$.[31] Due to the limited band width of the microwave pulses only selected orientations of the iron center with respect to the external magnetic field (θ_0, ϕ_0) are excited and contribute to the echo. Setting the external magnetic field to the g_3 or g_1 positions results in an excitation of a relatively narrow range of orientations, yielding a "single crystal"-like spectrum. At g_3 the centers with their z axis parallel to $\vec{H}$ are excited whereas at g_1 those with their x axis parallel to $\vec{H}$ are selected. In practice, one has to take into account a distribution around these orientations due to the band width of the pulse and the inhomogeneous EPR line width.

Figure 1 shows the three-pulse ESEEM waveforms recorded at a magnetic field of 2700 G ($g = 2.42$) of CP450($H_2{}^{17}O$), CP450(H_2O), and their ratio. The corresponding FT-ESEEM spectra are shown in Figure 2. The CP450(H_2O) spectrum consists of several lines below 7 MHz attributed to ^{14}N.[18,34] These ^{14}N peaks are not the subject of this work and will not be discussed any further. The peak at the proton Larmor frequency, 11.3 MHz, is due to weakly coupled protons, whereas

(29) McCracken, J.; Peisach, J.; Dooley, D. M.; *J. Am. Chem. Soc.* **1987**, *109*, 4064.
(30) Gunsalus, I. C.; Wagner, G. C. *Meth. Enzymol.* **1978**, *52*, 166.
(31) Lipscomb, J. *Biochemistry* **1980**, *19*, 3590.
(32) Thomann, H.; Bernardo, M. *Spectrosc. Int. J.* **1990**, *8*, 119.
(33) Fauth, J.-M.; Schweiger, A.; Brauschweiler, L.; Forrer, J.; Ernst, R. R. *J. Magn. Reson.* **1986**, *66*, 74.
(34) Peisach, J.; Mims, W. B.; Davis, J. L. *J. Biol. Chem.* **1979**, *254*, 12379.

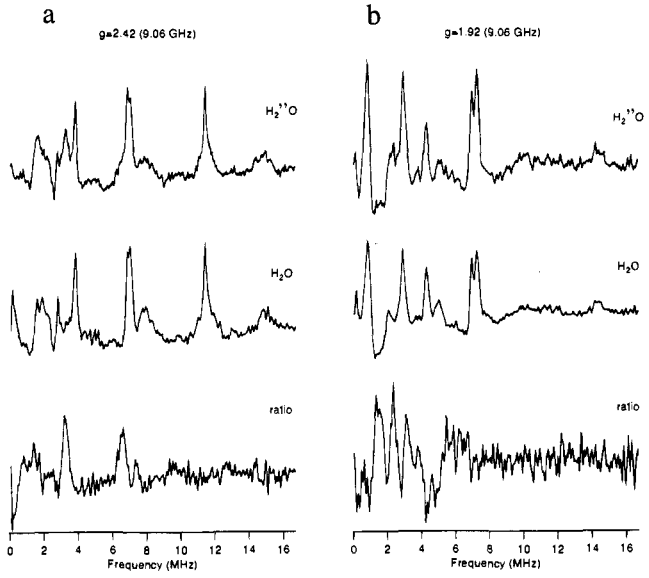

Figure 2. Three-pulse FT-ESEEM spectra of CP450($H_2{}^{17}O$) and CP450(H_2O) and their ratio recorded at a spectrometer frequency of 9.06 GHz, $\tau = 0.14$ μs: (a) $g = 2.42$ ($H_0 = 2700$ G), (b) $g = 1.92$ ($H_0 = 3400$ G).

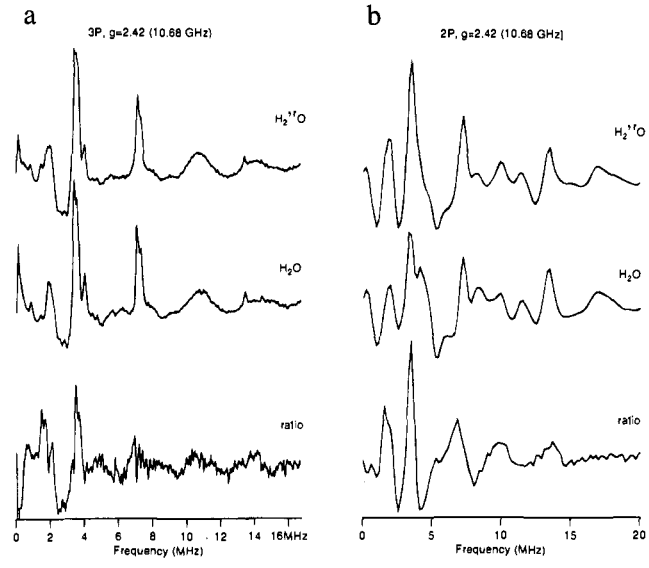

Figure 3. Two-pulse (b) and three-pulse (a) FT-ESEEM spectra of CP450($H_2{}^{17}O$) and CP450(H_2O) and their ratio recorded at a spectrometer frequency of 10.68 GHz and $g = 2.42$. The three-pulse ESEEM was recorded with $\tau = 0.21$ μs.

the doublet, at 7.8 and 14.8 MHz, centered about the proton Larmor frequency, is due to a strongly coupled proton(s).[18] It has been suggested that this doublet is either due to the S−H proton of the axial ligand[18] or due to protons of an axial water ligand.[18,19] The spectrum of CP450($H_2{}^{17}O$) looks very similar, although an additional peak at 3.2 MHz and a shoulder at 6.5 MHz are apparent. These peaks are well evident in the ratio spectrum. The absence of the strong ^{14}N peak at 3.77 MHz and of the proton peaks indicates that the ratio methodology is applicable for the three-pulse ESEEM as well. The three-pulse ESEEM spectra of CP450($H_2{}^{17}O$) and of CP450(H_2O) recorded at the high field end of the EPR spectrum, $H_0 = 3400$ G ($g = 1.92$), are shown in Figure 2b. The bottom spectrum, obtained from the ratio, differs significantly from that recorded at $g = 2.42$. It consists of four major peaks at 1.3−1.4, 2.3, 3.0, and 3.6 MHz and broad weak features between 5.5 and 6.5 MHz.

ESEEM experiments were carried out also at a higher spectrometer frequency, 10.68 GHz. The two-pulse FT-ESEEM spectra recorded at $g = 2.42$ ($H = 3153$ G) and their corresponding ratio spectrum are shown in Figure 3b. The ^{17}O spectrum consists of two relatively narrow lines at 1.56 and 3.51 MHz and broader peaks at 6.83, 9.7, and 13.6 MHz. The three-pulse FT-ESEEM spectra recorded at the same magnetic field with $\tau = 0.21$ μs, along with the ratio spectrum are shown in Figure 3a. The latter is very similar to the two-pulse spectrum showing two stronger peaks at 1.56 and 3.51 MHz and weaker, broader lines at 6.9, 10.4, and 13.8 MHz.

The ratioed ESEEM spectrum obtained from experiments carried out at g_2 showed very weak and broad peaks. The orientation selectivity is not as high at the g_2 position as at the g_1 and g_3 positions and many different orientations of the prosthetic group contribute to the echo. Unless the exact cancellation condition is met, excessive broadening is expected due to the large anisotropic quadrupole and hyperfine interactions.[35]

The Larmor frequency of ^{17}O at the magnetic fields applied is between 1.5 and 2 MHz. In none of the measurements was such a peak observed. This indicates that the hyperfine interaction is comparable to the nuclear Zeeman interaction. Weakly coupled water molecules within 4−6 Å of the Fe^{3+} are expected to contribute to the ESEEM line at the ^{17}O Larmor frequency. The absence of such a line indicates a disorder of the water molecules (with respect to the g-tensor principal axes) leading to an excessive broadening due to the quadrupole interaction.

^{17}O has a nuclear spin of $^5/_2$, thus in principle 10 fundamental modulation frequencies, 5 for each M_s manifold, corresponding to $\Delta M_I = \pm 1$ ENDOR transitions, are expected. The five frequencies in each of the M_s manifolds are split by the nuclear quadrupole interaction. If the quadrupole interaction is large enough, frequencies corresponding to $\Delta M_I = \pm 2$ are expected as well.[26] While the ESEEM spectrum recorded at g_1 is rather complex, that obtained at g_3 is simpler and can be used as a starting point in the spectrum analysis. The peaks at 1.3−1.4 and 3.2 MHz (see Figure 2a) may be attributed to a hyperfine doublet, given to first order by $\nu_{\alpha,\beta} = |\nu_I \pm a/2|$, where ν_I is the oxygen Larmor frequency and $a \approx 3$, and neglecting the quadrupole interaction. The peak at 6.4 MHz is then tentatively assigned to a $\Delta M_I = \pm 2$ overtone in the same manifold as the 3.2 MHz line. The latter is expected to be intense when a significant quadrupole interaction is present.[36] The low-frequency partner of the doublet is broader and harder to detect due to its larger sensitivity to the orientational disorder at this field position.

Further support for this assignment is obtained from spectra recorded at a spectrometer frequency of 10.68 GHz as shown in Figure 3. In these spectra the low-frequency partner of the doublet is more evident, particularly in the two-pulse spectrum. The high-frequency partner and the overtone are shifted by 0.3 and 0.4 MHz, respectively, with respect to the corresponding spectrum recorded at 9.06 GHz. Using the first-order expression for the nuclear frequencies, shifts of 0.26 and 0.52 MHz are expected. The relatively good agreement with the first-order expression suggests that at the particular orientations corresponding to the $g = 2.42$ position the effect of the ^{17}O quadrupole interaction is minimal, namely the component of $\mathbf{Q}$ along g_3 is very small. This suggests that $\eta \approx 1$ and that the direction of Q_{xx} is close to that of g_3.

The spectrum recorded at g_1 is more complex and cannot be analyzed using first-order arguments and requires spectral simulations. In the following section we present simulations

(35) Reijerse, E. J.; Keijzers, C. P. *J. Magn. Reson.* **1987**, *71*, 83.

(36) Matar, K.; Goldfarb, D. *Electron magnetic resonance of disordered systems (EMARDIS-91)*; Yordanov, N. D., Ed.; World Scientific: New York, 1991; p 273.

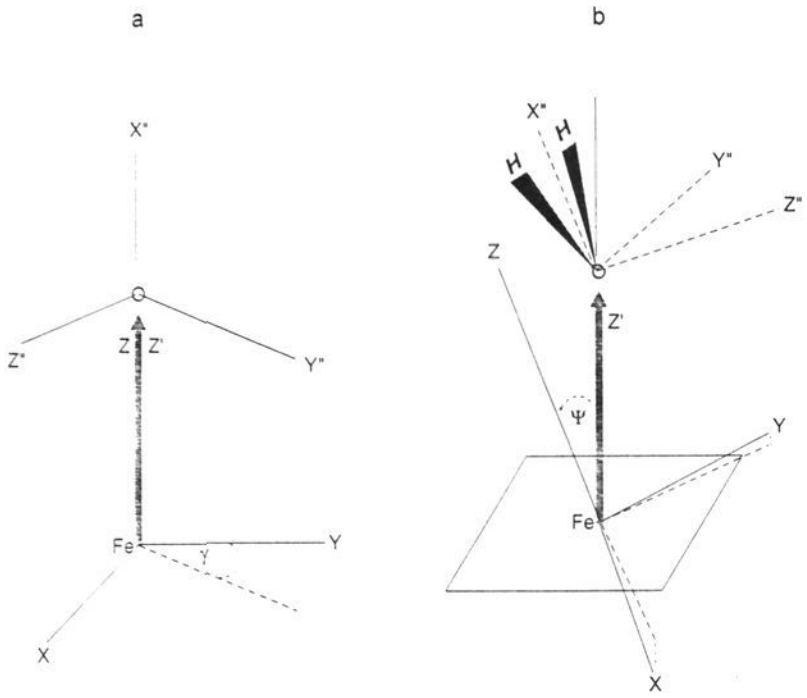

Figure 4. (a) A schematic representation of the principal axis system of the g-tensor (x, y, z) and the ^{17}O hyperfine (x', y', z') and the quadrupole (x'', y'', z'') tensors. (b) A schematic picture showing the orientation of the water molecule with respect to the heme plane and the corresponding tensor axes. ψ is the angle between the normal to the heme plane and the principal axis, z, of the g tensor.

which substantiate the above assignment of the $g = 2.42$ spectrum and are essential for the interpretation of the $g = 1.92$ spectrum. The simulations also provide information regarding the orientations and magnitude of the hyperfine and quadrupole tensors which in turn gives new insight to the nature of the distal axial ligand and the electronic structure of the CP450cam active site.

Simulations

In the following we present several sets of simulated spectra which demonstrate the characteristics of ^{17}O ESEEM spectra recorded at 2700 ($g = 2.42$) and 3400 G ($g = 1.92$) and show their dependence on the magnitudes and orientations of the hyperfine and quadrupole tensors. These series provide guide lines which indicate how the final best fit parameters were obtained and they establish the sensitivity of the spectra to the various spin Hamiltonian parameters involved. The simulations involve five parameters for the quadrupole interaction, e^2qQ/h, η, α, β, and γ, and four parameters for the hyperfine interaction, a_{iso}, $a_\perp$, θ_I and ϕ_I. We searched for one set of the best-fit parameters that will reproduce all four experimental spectra (Figures 2 and 3) which were recorded at different magnetic field values and at different microwave frequencies. Spectra recorded at $g = 2.42$ and g 1.92 will differ both in the oxygen Larmor frequency and in the range of selected θ_0 and ϕ_0 values. The simulations were calculated using an EPR line width of 50 G and principal g values of $g_1 = 1.92$, $g_2 = 2.242$, and $g_3 = 2.42$. These are slightly different from the previously reported values of $g_1 = 1.91$, $g_2 = 2.26$, and $g_3 = 2.45$.[31] This small change, however, has no effect on the general appearance of the spectra and the trends observed.

Our starting point was the spectrum recorded at $g = 2.42$, adapting the tentative assignment of the peaks described previously. Therefore, we took $\eta = 0.95$, x'' parallel to z ($\beta = 90°$, $\alpha = 0°$,) and $a_{iso} + 2a_\perp = 3.2$ MHz. A diagram showing the relative orientation of the g, A, and **Q** tensors is depicted in Figure 4a. Initially, the direction of the hyperfine interaction was assumed to be parallel to the Fe−O direction, perpendicular to the heme plane. Single-crystal EPR studies determined g_3 to be very close to the normal to the heme plane, thus $\theta_I \approx 0$.[37] This orientation also turned out to be the best fit orientation.

The effect of the size of e^2qQ/h on the three-pulse ESEEM

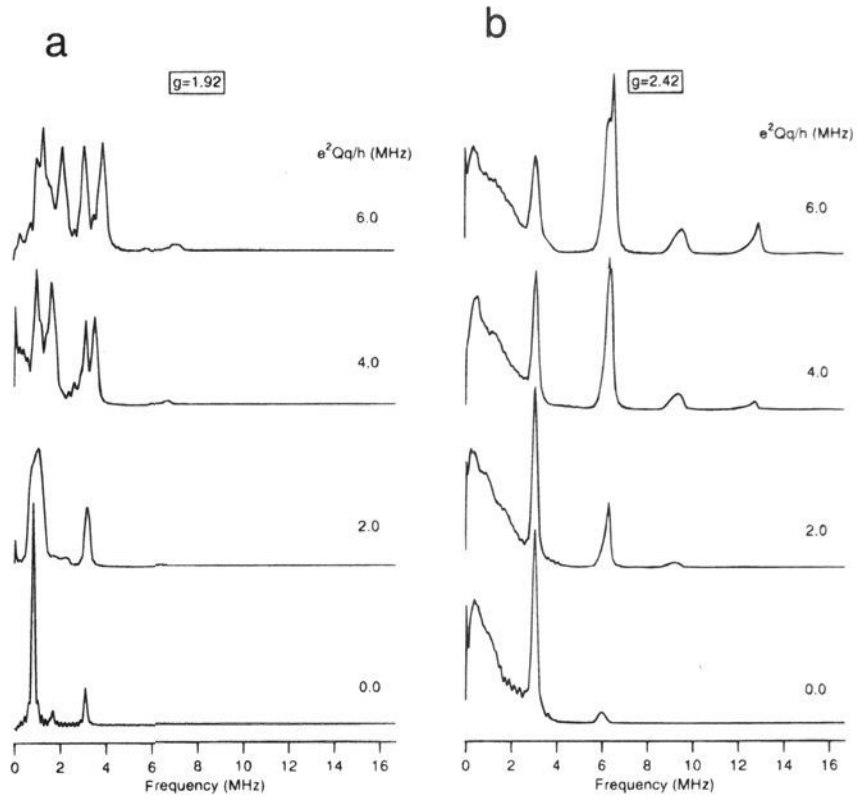

Figure 5. Calculated three-pulse ^{17}O FT-ESEEM spectra showing the effect of the quadrupole coupling constant, e^2qQ/h, on spectra obtained at $g = 2.42$ ($H_0 = 2700$ G) and at $g = 1.92$ ($H_0 = 3400$ G). Other parameters used in the simulations are the following: $a_{iso} = 2.6$ MHz, $a_\perp = 0.3$ MHz, $\theta_I = 0°$, $\phi_I = 0°$, $\eta = 0.95$, $\alpha = 0°$, $\beta = 90°$, $\gamma = 45°$, $\tau = 0.14$ μs.

spectrum calculated for $g = 2.42$ taking the quadrupole and hyperfine tensor orientations as discussed above, $a_{iso} = 2.6$ MHz and $a_\perp = 0.3$ MHz, is shown in Figure 5b. When $e^2qQ/h = 0$ the spectrum is dominated by the high-frequency hyperfine partner at 3.2 MHz and a weak overtone at 5.97 Mhz. The low-frequency hyperfine partner is broadened at this orientation due to the anisotropic hyperfine interaction. As e^2qQ/h increases the peaks broaden and shift slightly to higher frequencies, the intensity of the overtone significantly increases and higher order overtones start to appear at around 8.5 and 12.9 MHz. The relative intensity of the overtone peak at 6.3 MHz provides a means for determining the magnitude of the quadrupole coupling. Comparison with the experimental spectra indicates that it is within the range of 3−7 MHz.

The corresponding spectra calculated for $g = 1.92$ (3400 G) are shown in Figure 5a. When $e^2qQ/h = 0.0$ the spectrum consists of the two sharp hyperfine partners and a weak overtone of the low-field partner. The high-frequency line of the doublet is somewhat weaker due to the τ suppression effect. Unlike the $g = 2.42$ orientation, increasing e^2qQ/h introduces splittings in each of the hyperfine partners since at this orientation the magnetic field is along Q_{zz} which is large. When $e^2qQ/h = 6.0$ MHz, the spectrum is similar to the corresponding experimental spectrum with the exception of the peak at 3.88 MHz which is too intense and shifted by ≈0.28 MHz. Note also that the intensity of the $\Delta M_I = 2$ overtone is significantly smaller than in the spectra shown in Figure 5b since the magnetic field orientation is along z'' rather than x''.

Spectra similar to those presented in Figure 5a,b could be obtained by setting the hyperfine parameters to $a_{iso} = 0.4$ and $a_\perp = -1.8$ instead of $a_{iso} = 2.6$ and $a_\perp = 0.3$. Note that these two sets of hyperfine parameters yield almost identical hyperfine splittings along z and x (calculated from the first-order expression). The effects of a_{iso} and $a_\perp$ on the three-pulse ESEEM spectrum at $g = 2.42$ are shown in Figure 6a,b. The quadrupole tensor parameters used in these spectra are as in Figure 5a,b with $e^2qQ/h = 6.6$ MHz. The spectra shown were not

(37) Devaney, P. W. Thesis. Electron spin resonance study of single crystals of cytochrome P450 from pseudomonas putida. University of Illinois, Urbana, IL 1980.

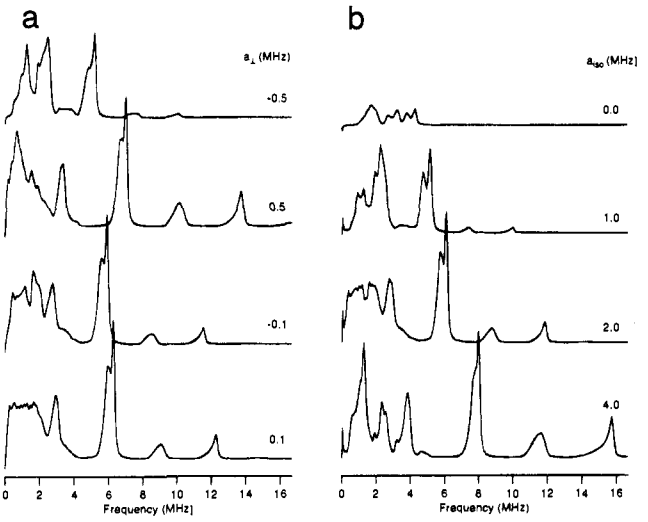

Figure 6. Calculated three-pulse ^{17}O FT-ESEEM spectra showing the effect of a_{iso} ($a_\perp = 0.3$ MHz) and $a_\perp$ ($a_{iso} = 2.6$ MHz) on spectra recorded at $g = 2.42$ and $H_0 = 2700$ G. Other parameters used in the simulations are the following: $\theta_I = 0°$, $\phi_I = 0°$, $e^2qQ/h = 6.6$ MHz, $\eta = 0.95$, $\alpha = 0°$, $\beta = 90°$, $\gamma = 45°$, $\tau = 0.14$ μs.

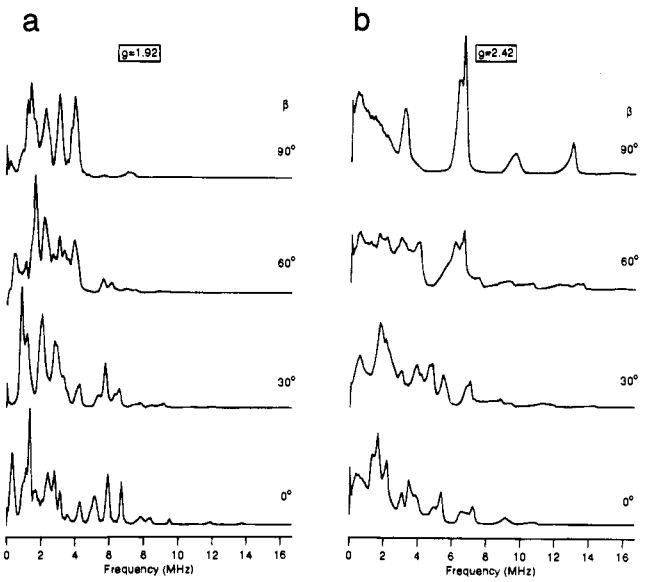

Figure 7. Calculated three-pulse ^{17}O FT-ESEEM spectra showing the effect of β on spectra obtained at $g = 2.42$ ($H_0 = 2700$ G) and at $g = 1.92$ ($H_0 = 3400$ G). Other parameters used in the simulations are the following: $a_{iso} = 2.6$ MHz, $a_\perp = 0.3$ MHz, $\theta_I = 0°$, $\phi_I = 0°$, $e^2qQ/h = 6.6$ MHz, $\eta = 0.95$, $\alpha = 0°$, $\gamma = 45°$, $\tau = 0.14$ μs.

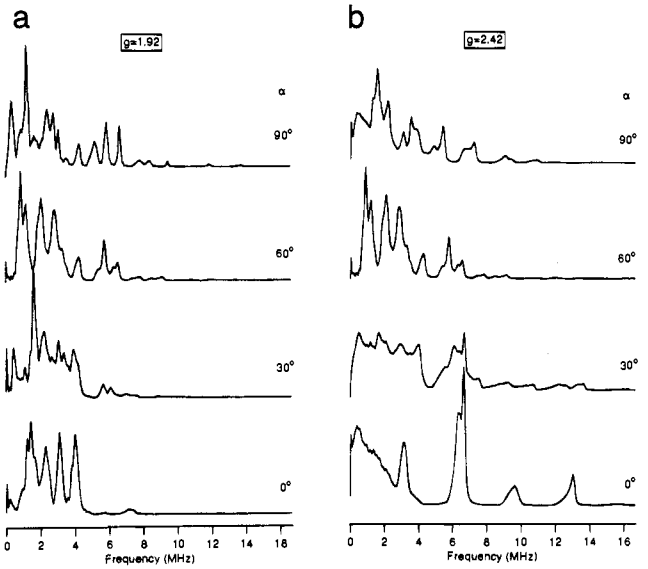

Figure 8. Calculated three-pulse ^{17}O FT-ESEEM spectra showing the effect of α on spectra obtained at $g = 2.42$ ($H_0 = 2700$ G) and at $g = 1.92$ ($H_0 = 3400$ G). Other parameters used in the simulations are the following: $a_{iso} = 2.6$ MHz, $a_\perp = 0.3$ MHz and (a) $a_{iso} = 2.6$ MHz, $a_\perp = 0.3$ MHz, $\theta_I = 0°$, $\phi_I = 0°$, $e^2qQ/h = 6.6$ MHz, $\eta = 0.95$, $\beta = 90°$, $\gamma = 45°$, $\tau = 0.14$ μs.

normalized; therefore, their relative intensities provide a direct measure of the modulation depth. In the series shown in Figure 6b, $a_\perp$ is held constant at 0.3 MHz and a_{iso} is varied. At $a_{iso} = 0$ three groups of lines appear. The first is approximately at the ^{17}O Larmor frequency, the second at 3.2 MHz, is probably due to a $\Delta M_I = 2$ overtone, and the 4.3 MHz group may arise from higher order overtones, shifted due to the quadrupole interaction. With increasing a_{iso} the modulation depth increases since the cancellation condition is approached,[35] the intensity of the overtones increases, and they shift to a higher frequency. $a_\perp$ also causes shifts of the lines, as shown in Figure 6a, where a_{iso} is held constant at 2.6 MHz. A positive $a_\perp$ shifts the peaks to higher frequencies whereas a negative value shifts them to lower frequencies. Obviously an opposite trend is expected if a_{iso} is negative rather than positive. The width and therefore the amplitude of the low frequency hyperfine partner at the $g = 2.42$ spectrum was found to depend on θ_I. When $\theta_I = 0-30°$ the width is broad as in the experimental spectrum, whereas at $\theta_I = 60-90°$ its magnitude becomes comparable to that of the high-frequency component.

It was mentioned earlier that in order to reproduce the $g = 2.42$ spectrum $\vec{H}$ has to be parallel to x'', namely $\beta = 90°$ and $\alpha = 0°$. This is illustrated in Figures 7b and 8b where the effects of β and α on the ^{17}O ESEEM spectrum are presented. Only when $\beta = 90°$ and $\alpha = 0°$ was it possible to obtain a spectrum dominated by two lines at 3.2 and 6.4 MHz. All other orientations generate spectra with a larger number of peaks due to significant quadrupolar splittings. The $g = 1.92$ spectrum is also highly sensitive to β and α as presented in Figure 7a and 8a. Due to the high value of η (≈ 1) similar spectra are obtained for different pairs of α and β, for instance 0, 90° and 90°, 0, respectively. When the value of η deviated significantly from 1 we could not find any combination of α and β which would reproduce the simple spectrum of $g = 2.42$.

Once β is set to 90° the $g = 2.42$ spectrum becomes practically invariant to changes in γ. This is expected since in this case a change in γ does not lead to a variation in the orientation of the external magnetic field with respect to z'' or x''. This, however, is not true for spectra recorded at $g = 1.92$ as the orientation of the external field with respect to the axes with large quadrupole components does change with γ. This is shown in Figure 9 for the two sets of hyperfine parameters which reproduce nicely the $g = 2.42$ spectrum. For both cases the simulated spectra with $\gamma = 45°$ exhibit better agreement with the experimental spectrum.

While the spectrum recorded at $g = 2.42$ could be reproduced rather easily determining e^2qQ/h, η, α, and β as well as the hyperfine splitting along z, more difficulties were encountered while fitting the $g = 1.92$ spectrum. As shown in the simulation series the latter is highly sensitive to all parameters set by the $g = 2.42$ spectrum and to γ. Therefore, this spectrum was used to determine γ and to refine the other parameters. In this case we initially tried to match the peak positions and then their relative intensities. In ESEEM spectroscopy the frequencies are generally more reliable and not affected by instrumental factors such as spectrometer dead time.

In all the simulations discussed above we have assumed that the axial ligand has a well-defined orientation with respect to

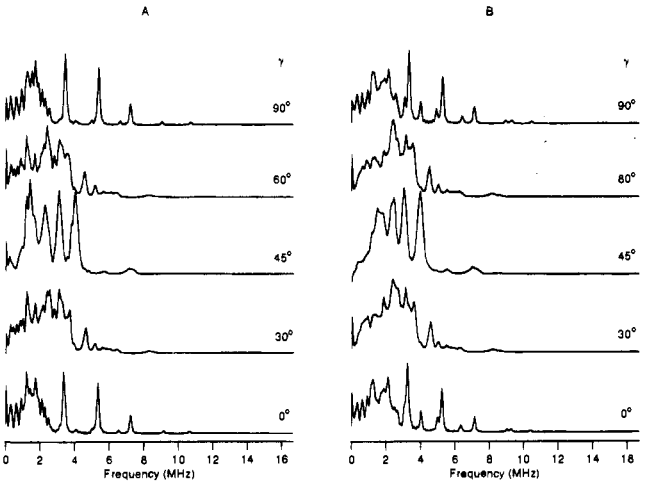

Figure 9. Calculated three-pulse ^{17}O FT-ESEEM spectra showing the effect of γ on spectra obtained at $g = 1.92$, $H_0 = 3400$ G and (A) $a_{iso} = 2.6$ MHz, $a_\perp = 0.3$ MHz and (B) $a_{iso} = 0.4$ MHz, $a_\perp = -1.8$ MHz. Other parameters used in the simulations are the following: $\theta_l = 0°$, $\phi_l = 0°$, $e^2qQ/h = 6.6$ MHz, $\eta = 0.95$, $\alpha = 0°$, $\beta = 90°$, $\tau = 0.14$ μs.

Table 1. Two Sets of Best Fit Parameters Used in the Simulations

	set A	set B
a_{iso}, $a_\perp$ (MHz)	$\pm 2.6 \pm 0.3$	$\pm 0.4 \mp 1.8$
θ_l(deg), ϕ_l (deg)	0.0, 0.0	0.0 0.0
e^2qQ/h (MHz), η	± 6.6, 0.95	± 6.6, 0.95
α, β, γ (deg)	0.0, 90, 50 $\pm$ 10	0.0, 90, 50 $\pm$ 10
EPR line width (G)	50	50

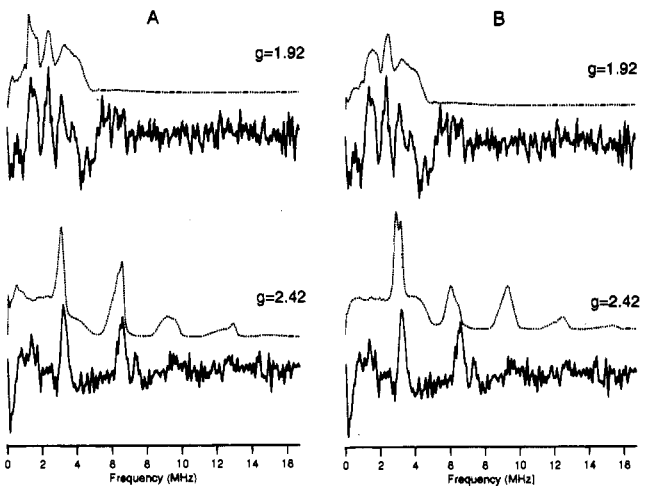

Figure 10. Calculated (dotted lines) three-pulse ^{17}O FT-ESEEM spectra obtained with the best-fit parameters listed in Table 1 for a spectrometer frequency of 9.06 GHz and the orientations (θ_0, ϕ_0) shown in Figure 4: (A) set A, (B) set B. The solid lines correspond to the experimental spectra (as in Figure 2).

the heme plane. This is not necessarily the case. It is possible that some disorder or rotation about the Fe−O axis occurs and is preserved upon freezing. In the case of complete disorder, γ can take any value between 0 and 180°. Simulated spectra calculated by averaging over γ did not agree with the experimental spectra. The fit with the experimental spectra could nevertheless be improved by taking $\gamma = 50 \pm 10°$. Spectra obtained with such a γ distribution and the two sets of hyperfine parameters listed in Table 1 are shown in Figure 10A,B. For direct comparison, the experimental spectra are also shown. The spectra obtained with $a_{iso} = 2.6$ MHz and $a_\perp = 0.3$ MHz agree somewhat better with the experimental spectra although the 6.5-MHz peak in the $g = 2.42$ spectrum is too intense. Its intensity can be reduced by decreasing e^2qQ/h but this improvement in the $g = 2.42$ spectrum will lead to an undesirable severe change

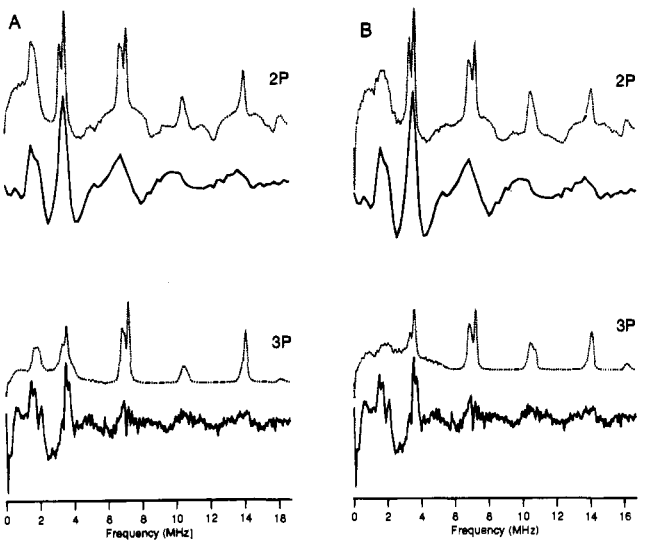

Figure 11. Calculated (dotted lines) two- (top) and three-pulse (bottom) ^{17}O FT-ESEEM spectra ($\tau = 0.21$ μs) obtained with the best-fit parameters listed in Table 1 for a spectrometer frequency of 10.68 GHz and $g = 2.42$. The selected orientations, θ_0 and ϕ_0, were calculated using the principal g values as in Figure 4: (A) set A, (B) set B. The solid lines correspond to the experimental spectra (as in Figure 3).

in the spacing between the lines in the $g = 1.92$ spectrum. Increasing the ranges of θ_0 and ϕ_0, assuming an inhomogeneous line width of 80 G rather than 50 G, did not introduce significant improvement in the fit for either the $g = 2.24$ nor the $g = 1.92$ excitations.

A comparison of the simulated two-pulse and three-pulse ESEEM spectra using the parameters listed in Table 1 and a spectrometer frequency of 10.68 GHz and $g = 2.42$ to the experimental results is shown in Figure 11A,B. While the calculated spectra reproduce the positions of all peaks observed experimentally, the width of the overtones is significantly greater in the experimental spectra. For $a_{iso} = 2.6$ MHz and $a_\perp = 0.3$ MHz the overtone at 7.0 is too intense whereas for $a_{iso} = 0.4$ MHz and $a_\perp = -1.8$ MHz the peak at 1.5 MHz is too weak. Based on the available experimental results and the simulations performed, we cannot remove the degeneracy of the two possible sets of hyperfine parameters. The simulations were sensitive to the relative signs of a_{iso} and $a_\perp$ but not to their absolute signs. Similar calculated spectra were obtained for a_{iso} and $a_\perp$ of -2.6 and -0.3 MHz and -0.4 and 1.8 MHz, respectively.

Discussion

The ^{17}O ESEEM results provide direct evidence for the existence of an axial oxygen containing ligand and thus agree with the X-ray results.[5] While our simulations did not generate an unambiguous solution for the hyperfine parameters, the quadrupole tensor parameters were determined uniquely and with no ambiguity, with an estimated error of $\pm 10\%$. These parameters could be more easily determined due to the large asymmetry parameter and the special relative orientation of the g and Q tensors which yield a unique spectrum at $g = 2.42$. The ^{17}O quadrupole tensor parameters we obtained are similar to those of ^{17}O in water and of particular interest is the large asymmetry parameter, which is close to unity.[38,39] Similar coupling constants and large asymmetry parameters were observed for barium chlorate monohydrate ($e^2qQ/h = -7.61$ MHz, $\eta = 0.94$)[40] and sodium tetrachloroaurate dihydrate

(38) Brosnan, S. P. G.; Edmonds, D. T. *J. Mol. Struct.* **1980**, *58*, 23.
(39) Verhoeven, J.; Dymanus, A.; Bluyssen, H. *J. Chem. Phys.* **1969**, *50*, 3330.
(40) Shporer, M.; Achlama, A. M. *J. Chem. Phys.* **1976**, *65*, 3657.

($e^2qQ/h = -7.79$ MHz, $\eta = 0.87$).[41] A single crystal ENDOR study of $H_2{}^{17}O$ ligated to Mn^{2+} doped in La $Mg(NO)_2)_{12}$·$24H_2O$ gave $e^2Qq/h = 7.4$ MHz and $\eta = 0.79$.[42] Similar values were also used to simulate ENDOR spectra of $Mn(H_2{}^{17}O)_6{}^{2+}$ in a frozen solution.[43] In all these cases the z'' axis was found to be perpendicular to the HOH plane. In the case of potassium hydrogen maleate, where a hydrogen-bonded OH^- is involved, $\eta = 0.589$, and the z'' axis makes an angle of 60° with the OH direction.[44] Based on the high value of η in our system we conclude that the oxygen-containing ligand is a water molecule and not an OH^- group. Unlike OH^-, water is a weak ligand, which implies that probably the other ligands act as strong ligands and only a very small additional change in energy is required for the transformation to the low-spin state. This small change is provided even by a weak ligand such as water.

In addition to the quadrupolar coupling constant and the asymmetry parameter, the simulations performed also yield the orientation of the quadrupole tensor with respect to the principal axis system of the g matrix. Single-crystal EPR results[37] combined with the available crystal structure[5] showed that the largest g component, g_3, is approximately along the normal to the heme plane (18 ± 3°) and the other two principal axes are nearly in the heme plane.[3] Accordingly, the values $\alpha = 0°$, $\beta = 90°$, and $\gamma = 50 \pm 10°$ indicate that the water molecule is oriented with its HOH bisector almost parallel to the heme normal (tilted by 18 ± 3°) as is schematically shown in Figure 4b. Moreover, at low temperatures the orientation of the water molecule with respect to the x,y direction is well-defined, as manifested by the value of γ (50 ± 10°). Namely, the orientation of the water molecule is confined with respect to the Fe−N directions in the heme. Unfortunately, we could not determine the orientation of the HH vector in the water molecule with respect to the Fe−N directions in the heme plan since we could not identify from the single crystal work[37] the direction of the x,y axes with respect to the crystal axes as given in the X-ray structure.[5]

The simulations showed that two sets of hyperfine parameters (see Table 1) yield spectra that reproduce satisfactorily the experimental results. The difference in the agreement between simulations and experiment for these two sets of hyperfine parameters is minor and well within the accuracy of the results. In both cases the isotropic hyperfine interaction is rather small, ±2.6 or ±0.4 MHz. For comparison, in high-spin aquomet-myoglobin the ^{14}N isotropic hyperfine coupling for the axial histidine residue is 9.3 MHz.[46] This is attributed to a significant population of unpaired spin density in the d_{z^2} orbital involved in σ bonding with the axial ligand. Similarly, in frozen solutions of $Mn(H_2{}^{17}O)_6{}^{2+}$ a_{iso} and $a_\perp$ were found to be −7.5 and −1.2 MHz, respectively.[43] The larger value for a_{iso} is again attributed to the fact that Mn^{2+} has a d^5, $S = {}^5/_2$, configuration in which there is a significant spin density in the d_{z^2} orbital which is involved in the σ bond with the axial ligand.

In low-spin CP450 the ground state electronic structure is comprised of the partially filled t_{2g} orbitals, d^2_{xy}, d^2_{xz}, d^1_{yz}, and an empty e_g set.[45] The degeneracy of the t_{2g} orbitals is removed by the tetragonal distortion induced by the different in-plane and axial ligands and by additional rhombic splitting due to the proximal axial ligand. The d_{z^2} orbital can gain a small unpaired spin density through spin−orbit coupling which mixes the d_{yz} and d_{z^2} orbitals. Two mechanisms for obtaining finite spin density on the axial oxygen ligand are by direct orbital overlap and exchange polarization.

For the electronic configuration of low-spin CP450, the spin density on the axial oxygen arising either from direct overlap by σ and/or π bonding or by exchange polarization is expected to be very small. The presence of the cysteine proximal ligand may also lead to some reduction in the hyperfine coupling on oxygen by the so-called trans effect. This refers to the reduction in the hyperfine coupling by delocalization of spin density on to the trans axial ligand. For instance, the hyperfine coupling of the pyridine nitrogen in the low-spin complex heme(pyridine)-(2-mercaptoethanol) and of the axial nitrogen in heme(propylamine)(2-mercaptoethanol) was found to be about 2 MHz.[46] These values are lower than the 4−5 MHz values reported for bound axial nitrogens in a low-spin heme or porphyrins with a proximal imidazole ligand rather than a mercapto ligand.[47,48] For the present case of low-spin CP450, the negligible difference between the ^{17}O quadrupole coupling constant with respect to ice suggests that donation from the oxygen lone pair into the empty Fe d_{z^2} orbital is minimal which is consistent with the very small hyperfine couplings.

Spin density transfer from the metal to the ligand could be obtained by direct overlap of the partially filled metal d_π orbital with one of the filled oxygen p_π orbitals. If the water molecule is situated so that the lone-pair electrons in the oxygen a_1 orbital are pointing into the empty d_{z^2} orbital, the lone pair electrons in the oxygen b_1 orbital can overlap with the partially filled Fe d_{yz} orbital. This π bonding would place unpaired spin density on to oxygen but does not account for the finite a_{iso} since the out-of-plane oxygen p_y orbital has little or no s character. The Euler angles for the ^{17}O quadrupole interaction indicate that the tilting of the HOH plane away from the normal to the heme plane is small. Some s character could be introduced by mixing of the a_1 and b_1 orbitals associated with the small tilting of the HOH plane away from the normal to the heme plane. The small 2s character of such a molecular orbital would lead to a (small) negative a_{iso} (taking into account the negative gyromagnetic ratio of ^{17}O). This constraint on the sign of a_{iso} requires that for fit parameters set B (see Table 1), $a_\perp = +1.8$ MHz while for set A, $a_\perp = -0.3$ MHz.

The second mechanism for obtaining finite spin density on the axial oxygen ligand is by exchange polarization between the lone pair electrons in the oxygen a_1 orbital and finite spin density in the Fe d_{z^2} orbital. (The d_{z^2} orbital can gain a small unpaired spin density through spin−orbit coupling which mixes the d_{yz} and d^2_z orbitals.) Since the oxygen b_1 orbital has finite s character, this mechanism naturally accounts for the finite Fermi contact coupling on the oxygen. The exchange polarization mechanism should lead to a negative spin density on the oxygen and thus to a positive a_{iso}. This constraint on the sign of a_{iso} requires that for fit parameters set B (see Table 1), $a_\perp = -1.8$ MHz while for set A, $a_\perp = +0.3$ MHz.

For a Fe−O distance of 2−2.28 Å the point dipole approximation gives $a_\perp = -(0.9-1.4$ MHz) assuming $g = 2$. (The negative sign is due to the negative magnetogyric ratio of ^{17}O.) To the extent that the point-dipole approximation is applicable, it can be used to discriminate between the sets of best-fit parameters. Given the uncertainties in the experimental values and the uncertainties in the values determined from the best-fit simulations, it appears that either of the two mechanisms, i.e., direct overlap or exchange polarization, would be consistent

(41) Achlama, A. M. *Chem. Phys. Lett.* **1977**, *48*, 501.
(42) Glotfelty, H. W. Thesis. A ^{17}O study of cobalt and manganese hydrated complexes of some double nitrates. University of Kansas, Lawrence, KS, 1978.
(43) Tan, X.; Bernardo, M.; Thomann, H.; Scholes, C. P. *J. Chem. Phys.* **1995**, *102*, 2675.
(44) Poplett, I. J. F.; Smith, J. A. S. *J. Chem. Soc., Faraday Trans. 2* **1979**, *75*, 1703; *J. Mol. Struct.* **1980**, *58*, 1.
(45) Taylor, C. P. S. *Biochem. Biophys. Acta* **1977**, *491*, 137.
(46) Peisach, J.; Mims, W. B.; Davis, J. L. *J. Biol. Chem.* **1979**, *254*, 12379.
(47) Magliozzo, R. S.; Peisach, J. *Biochemistry* **1992**, *31*, 189.
(48) Scholes, C. P.; Falkowski, K. F.; Chen, S.; Bank, J. *J. Am. Chem. Soc.* **1986**, *108*, 1660.

with the experimental results. In the case of the direct overlap mechanism, hyperfine parameter set A with $a_\perp = -0.3$ MHz is within the acceptable limit of uncertainty. In the case of the exchange polarization mechanism, hyperfine parameter set B with $a_\perp = -1.8$ MHz is within range.

Further insight into the origin of the hyperfine interaction may be achieved by decomposing the hyperfine interaction into the following components:[49]

$$A_{xx} = a_{iso} - A_{dd} - A_\sigma + 2A_\pi$$

$$A_{yy} = a_{iso} - A_{dd} - A_\sigma - A_\pi$$

$$A_{zz} = a_{iso} + 2A_{dd} + 2A_\sigma - A_\pi \quad (6)$$

where a_{iso} is proportional to the unpaired electron population in the oxygen s orbital, A_{dd} is the direct dipole−dipole interaction with the unpaired electron on the Fe, A_σ is the contribution to the dipole−dipole interaction with unpaired electron in an oxygen p orbital involved in a σ bond, and A_π is the contribution to the dipole−dipole interaction with unpaired electron spin density in the p_π orbital, perpendicular to the HOH plane. Inspection of eq 6 shows that an axially symmetric hyperfine interaction will only be obtained if A_π is negligible. The direct overlap of the partially filled metal d_π orbital with one of the filled oxygen p_π orbitals would result in a large anisotropic hyperfine component parallel to the heme plane and in a non-axial hyperfine tensor. This is obviously not consistent with our initial assumption that the hyperfine interaction is axially symmetric. This initial assumption was a first-order estimate motivated by its simplicity and ultimately rationalized by the quality of the fits between the simulated and experimental spectra. It is likely that a non-axial hyperfine interaction would further improve the quality of the fits since there are more adjustable parameters. However, this also exascerbates the problem of determining the uniqueness of the fit parameters.

Inspection of eq 6 shows that an anisotropic hyperfine component smaller than A_{dd} can exist only if the contributions of A_σ and/or A_π are significant. If we assume that A_π is negligible so that the hyperfine interaction is axially symmetric, we are left with the two possibilities that either $A_\sigma \ll A_{dd}$ and A_σ is of the same sign as A_{dd} or that $A_\sigma \simeq A_{dd}$ but has an opposite sign. These two possibilities correspond to the fit parameters set B and set A, respectively. Since the Fe−O direction is along the z axis, both A_{dd} and A_σ are at their maximum values and both are negative. This simple ligand field analysis and the constraint of an axially symmetric hyperfine interaction leads to the conclusion that the spin transfer mechanism is by exchange polarization and that the fit parameters set B, with $a_{iso} = +0.4$ MHz and $a_\perp = -1.8$ MHz, are more plausible than those of set A. An exchange polarization mechanism was also proposed to account for the ^{14}N hyperfine interaction in the proximal axial imidazole ligand in low-spin myoglobin hydroxide and in a series of Fe^{3+} tetraphenylporphrin complexes.[47] In the latter the a_{iso} of ^{14}N was determined to be negative whereas $a_\perp$ was positive. Similar results were also observed for ferric low-spin bis(imidazole)ligand heme systems.[48] However, it is clear from Figure 11 that the ESEEM frequencies of the fit with parameter set A are slightly better than the fit obtained for parameter set B. We therefore speculate that the hyperfine interaction is in fact not axially symmetric. In this case, we are not able to deduce which ligand field model is applicable based only on the spin Hamiltonian parameters that are determined from these experiments. Guidance from *ab initio* or semiempirical electronic structure calculations is needed.

Finally we note that our results indicate the presence of one type of water ligand which is in disagreement with a recent interpretation of proton ENDOR results.[19] Combined orientation selective ^1H four-phase ESEEM and ^1H pulse ENDOR results we have recently obtained confirm our present interpretation.[50]

Conclusions

Using ^{17}O ESEEM we confirmed the presence of an oxygen-containing axial ligand in low-spin native CP450cam and provided direct evidence that at pH 7.5 this ligand is a water molecule rather than an OH^-. Moreover, from the orientation of the ^{17}O quadrupole tensor, the orientation of the water molecule was found to be confined (within ±10°) with respect to the Fe−N directions within the heme plan. The small ^{17}O hyperfine couplings obtained are consistent with the unpaired electron being predominately in the d_{yz} orbital. The fact that the fact water ligand is not randomly oriented indicates that either orbital overlap constrains the orientation of the ligand or that the orientation is dictated by hydrogen bonding to nearby protein side chain residues or to other water molecules.

Acknowledgment. We thank Dr. G. C. Wagner for providing the cytochrome P450cam starting material and the Stable Isotope Resource at Los Alamos National Laboratory for providing the ^{17}O-enriched water (supported by NIH Grant No. RR02231, under the auspices of the US Department of Energy). We also thank Dr. H. Beinert for his continuous interest and encouragement of this work.

JA9508986

(49) Scholes, C. P.; Lapidot, A.; Mascarenhas, R.; Inubushi, T.; Isaacson, R. A.; Feher, G. *J. Am. Chem. Soc.* **1982**, *104*, 2724.

(50) Goldfarb, D.; Bernardo, M.; Thomann, H.; Kroneck, P. M. H. In preparation.